SOA Intensity Noise Suppression in Spectrum Sliced Systems: A Multicanonical Monte Carlo Simulator of Extremely Low BER

Amirhossein Ghazisaeidi, Francesco Vacondio, Alberto Bononi, and Leslie Ann Rusch, *Senior Member, IEEE*

***Abstract*—We present a thorough numerical study of intensity noise mitigation of spectrum sliced wavelength-division multiplexing (SS-WDM) systems employing a nonlinear semiconductor optical amplifier (SOA) before the modulator. Our simulator of the SS-WDM link, embedded inside a Multicanonical Monte Carlo (MMC) platform, estimates the tails of the probability density functions of the received signals down to probabilities smaller than 10^{-16}. We introduce a new, simple, and efficient technique to handle intersymbol interference (ISI) in MMC simulations. We address the impact of optical postfiltering on SOA noise suppression performance. While previous research experimentally observed the SOA-induced noise cleaning in SS-WDM systems, this is the first complete simulator able to correctly predict the ensuing BER improvement. We measure the BER at different bit-rates and validate predicted BERs with and without post filtering.**

***Index Terms*—ISI, modeling, multicanoncial Monte Carlo, noise suppression, SS-WDM, SOA.**

I. Introduction

INTENSITY noise suppression of spectrum-sliced wavelength-division multiplexing (SS-WDM) systems by semiconductor optical amplifiers (SOAs) operating in deep saturation has been the subject of several studies in recent years [1]–[12]. Compared to other noise suppression techniques [13]–[15], SOA-based noise suppression is interesting due to its efficiency and ease of implementation, as well as its potential for a solution in integrated optics. It has also been utilized in 2R regenerators for long-haul transmission systems [16], [17], and to reduce the mode partition noise of semiconductor lasers [18].

While SOA-based intensity noise mitigation has been studied extensively both experimentally and theoretically, no general-purpose design tool exists to optimize the bit error rate (BER) performance for a desired SOA-based system. For example, for a given SOA technology and modulation format what postfiltering bandwidth yields the lowest BER? Does this change with a more complex modulation format? What SOA design parameters have the greatest impact on the noise mitigation performance? The major contribution of this paper is to provide a tool to answer such questions.

The exact form of the photon statistics at the output of a nonlinear amplifier is extremely complicated to derive [19]. In the case of saturated SOAs two approximate approaches exist: 1) characterizing the noise spectra at the SOA output whether the source is coherent [20] or incoherent [4], and 2) analytical approximations of the probability density function (PDF) of the output intensity when the source is coherent [21]. In the first approach the noise spectrum at the SOA output is calculated for continuous-wave (CW) input light. This method is useful in that it determines the suppression bandwidth, and provides an estimate of the relative intensity noise (RIN) reduction. However, it does not provide the indispensable knowledge of the PDF of the output intensity for a complete statistical analysis.

In [21], a PDF is obtained when the source is coherent using perturbation theory; the ASE field added to the coherent signal is treated as a perturbation. Analytical expressions for the PDF are derived using path-integral methods. However, the perturbation approach to find the PDF cannot be extended to incoherent sources whose optical field is a zero mean process. In summary, to date we can find the RIN spectrum of the photodetected signals when the source is CW, either coherent or incoherent; or we can find the PDF of the SOA output light intensity (and, hence, find the BER) when the SOA input is coherent CW. In either case the analysis is limited to continuous-wave only. The impact of modulation, for example through the induced patterning effects in the amplifier [22], is not captured. Our simulator fills these gaps.

Our interest in noise statistics is applied in particular to noise suppression properties of a SOA on incoherent light in SS-WDM systems. In those systems, as demonstrated by McCoy, *et al.* [10], [11], optically filtering the received signal by a channel selecting filter (CSF) at the receiver side results in significant neutralization of the intensity noise suppression. Although the phase-to-intensity conversion due to optical filtering signals with noisy phase is treated in [23] for coherent sources, no quantitative analysis of the postfiltering in the case of SS-WDM exists in the literature. Our simulator includes not just the SOA, but the complete SS-WDM system in order to capture this important phenomenon.

Given the insurmountable hurdles discussed for an analytical attack, numerical techniques are favored to study the statistical properties of nonlinearly amplified spectrum slices. Since a SOA is a nonlinear element with memory, standard semi-analytical methods for additive Gaussian noise [24] are not applicable; we must resort to Monte Carlo (MC) simulations. Numerical

Manuscript received May 29, 2008; revised September 29, 2008. Current version published July 01, 2009. This work was supported by the 2007-2009 Quebec-Italy Executive Program for Scientific Development, Project 13.

A. Ghazisaeidi, F. Vacondio, and L. A. Rusch are with the ECE Department, COPL, Université, Laval, Quebec, QC, CA (e-mail: rusch@gel.ulaval.ca).

A. Bononi is with the Dipartimento di Ingegneria dell'Informazione, Universita di Parma, 43100 Parma, Italy.

Color versions of one or more of the figures in this paper are available online at http://ieeexplore.ieee.org.

Digital Object Identifier 10.1109/JLT.2009.2014787

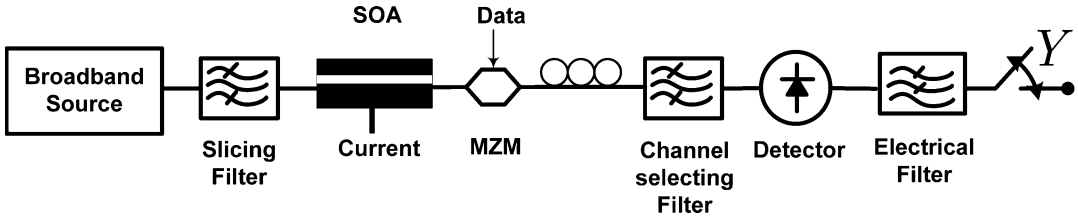

Fig. 1. SS-WDM link equipped with a premodulator noise suppressing SOA. MZM: Mach–Zehnder modulator, Y: sampled received voltage.

PDF estimation of links including nonlinear amplifiers, however, requires prohibitive computation time. It is well-known that in estimating the probability of an event by MC simulation, if p is the (unknown) desired probability and $\hat{p}$ is its estimate, and if N samples are generated in an MC simulation, we have $\mathrm{var}\{\hat{p}\}/\mathrm{E}^2\{\hat{p}\} = 1/Np$, where $\mathrm{E}\{\cdot\}$ stands for expectation, i.e., the relative estimation error is given by $1/\sqrt{N \cdot p}$. If the target event is the bit error rate, generating $N = 10^{10}$ samples results in 33% relative error in estimating a $\mathrm{BER} = 10^{-9}$ [25]. As an example, at 2.5 Gb/s, and using a fourth-order Runge–Kutta method to solve the Agrawal SOA equations [26] (the lowest-complexity dynamic SOA model) MC simulations might require days to estimate a BER $\sim 10^{-9}$. Even worse, the more accurate space-resolved SOA model used in this paper, to achieve an accurate match to experimental results, requires a simulation time two orders of magnitude larger than that of the simple Agrawal SOA model.

To overcome this huge computational burden, we use the Multicanonical Monte Carlo (MMC) simulation method [27]. The application of MMC in optical communication has been discussed by several authors [28]–[34]. In particular, MMC was used to study the statistical properties of a coherent laser pulse amplified by a saturated SOA [35], [36]. Our contribution to the extension of these MMC methods is twofold: an extension to incoherent light and modeling of intersymbol interference.

We present a statistical characterization of SOA-based noise suppression and BER estimation in SS-WDM systems using an incoherent source, which is, to the authors' knowledge, new in the literature. We model incoherent light, in the time domain, as a signal whose complex envelope is a zero-mean Gaussian process [37]. This process is filtered optically in our numerical simulations; the level of coherence of the output light depends on the spectral characteristics of the filter.

We present a general MMC platform. We introduce a new, simple and efficient technique to handle the intersymbol interference (ISI) in MMC simulations. We believe our simulator can be used to study the performance of a large variety of optical links employing nonlinear amplifiers, especially various SOA-based regenerators. The organization of the paper is as follows. In Section II, we discuss the theory of SOA-based noise suppression. In Section III, we describe the simulator. In Section IV, we give the numerical and experimental results, and in Section V, we conclude. We give details of the MMC algorithm in the Appendix.

II. SOA Noise Suppression Mechanism

Fig. 1 shows an SS-WDM link equipped with a premodulator noise-suppressing SOA. The optical field after the slicing filter is a band-limited, complex Gaussian random process. The source intensity at each instant has a negative exponential distribution, resulting in 0 dB of source relative intensity noise. Such a large intensity noise introduces a BER floor that severely limits the performance of SS-WDM. A SOA operating in saturation placed before the modulator offers considerable intensity noise mitigation due to self gain modulation [11], [14], [20].

The propagation equation of the optical field inside a traveling-wave SOA in the moving frame is [20]

$$\frac{\partial S(z,t)}{\partial z} = \frac{1}{2}[(1-j\alpha)g(z,t) - \beta(z,t)]S(z,t) + \varepsilon(z,t) \quad (1)$$

where $S(z,t)$ is the optical field, z is position along the longitudinal axis of the SOA waveguide, t is time in the moving frame, $g(z,t)$ is the SOA material gain, $\beta(z,t)$ is the SOA loss coefficient, α is the linewidth enhancement factor, and $\epsilon(z,t)$ is a random process modeling the spontaneous emission inside the SOA waveguide. The material gain is given by

$$g(z,t) = \Gamma a(N(z,t) - N_T) \quad (2)$$

where $N(z,t)$ is the carrier density, Γ is the confinement factor, a is the differential gain, and N_T is the transparency carrier density. The loss coefficient is

$$\beta(z,t) = K_0 + \Gamma K_1 N(z,t) \quad (3)$$

where K_0 and K_1 are the carrier independent loss coefficients [38]. Using (2) in (3), we get

$$\beta(z,t) = \beta_0 + \beta_1 g(z,t) \quad (4)$$

where $\beta_0 \triangleq K_0 + \Gamma K_1 N_T$ and $\beta_1 \triangleq \Gamma K_1/a$.

The spontaneous emission is modeled by the well-known Langevin force terms [35], and can be written as

$$\varepsilon(z,t) = \frac{\hbar\omega_0}{2}\sqrt{g(z,t) + \Gamma a N_T}(n_r(z,t) + jn_i(z,t)) \quad (5)$$

where ω_0 is the central optical frequency, and $n_r(z,t)$, and $n_i(z,t)$ are independent zero-mean white Gaussian noise random processes. The dynamic gain equation is [20]

$$\frac{\partial g(z,t)}{\partial t} = \frac{g_0 - g(z,t)}{\tau_c} - g(z,t)\frac{|S(z,t)|^2}{\tau_c P_{\mathrm{sat}}} \quad (6)$$

where τ_c is the SOA carrier lifetime, and P_{sat} is the SOA saturation power. The parameters of the SOA we used in this work are listed in Table I.

According to (6), at each z and t, the SOA gain inversely follows fluctuations of the optical intensity; if the light intensity increases, the gain decreases, and the increased intensity experiences decreased gain in subsequent instants. Similarly, a decrease in the light intensity allows the gain to recover; thus, a

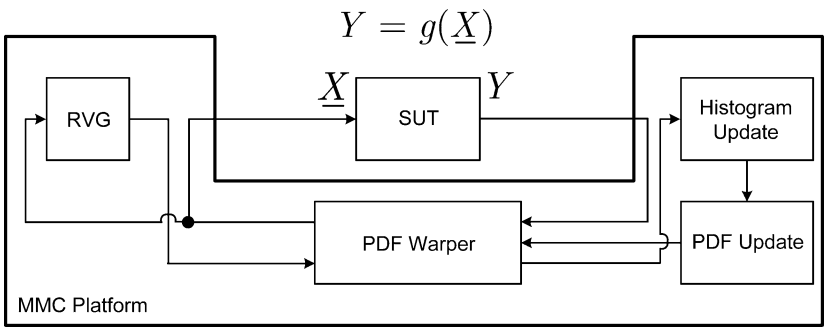

Fig. 2. MMC platform. RVG: random vector generator, SUT: system under test.

TABLE I
SOA PARAMETERS USED IN SIMULATIONS

Carrier lifetime, τ_c	170 ps
Saturation power, P_{sat}	14 dBm
Linewidth enhancement factor, α	3.5
small signal gain, g_{ss}	14500 $1/m$
Carrier independent loss coefficient, β_0	2180 $1/m$
Carrier dependent loss coefficient, β_1	1600 $1/m$
SOA length, L	650 μm
$\hbar\omega_0$	1.28e-19 J
$\Gamma a N_T$	70001$/m$

decreased intensity experiences a greater gain. This self gain modulation mechanism reduces the relative intensity noise of the SOA output compared to its value at the input. However, the $1/\tau_c$ dependence in (6) indicates the SOA gain cannot respond to light fluctuations faster than the carrier recombination rate $1/\tau_c$. The RIN spectrum of amplified CW light has a high-pass response (i.e., a DC dip) as fluctuations slower than the SOA active region response time are suppressed, while those above the suppression bandwidth remain.

The preceding discussion qualitatively explains the physical origin of SOA-based noise suppression. The detailed quantitative treatment is given in [4] and [20], where expressions for noise spectra are calculated for the CW coherent and incoherent sources respectively. In the following sections we use (1)–(6), and parameters given in Table I, to form a space-resolved model for the SOA. The SOA model is a part of a larger one for the the SS-WDM link of Fig. 1, which will be simulated inside an MMC platform to estimate the PDF of the sampled output signal Y (see Fig. 1).

III. SYSTEM SIMULATOR

In this section, we give a top-down description of the simulator. In the next subsection we discuss the MMC platform, while a description of the MMC algorithm is given in the Appendix. In Section III-B, we discuss the model of the optical link, and in Section III-C, we discuss the SOA model.

A. MMC Platform

MMC simulation method [27] is an adaptive importance sampling that requires minimal *a priori* knowledge of the system under test (SUT). It consists of a predetermined number of cycles, the first of which is a short MC simulation of the SUT. Learning from the histogram of the output samples of the SUT at the end of each cycle, MMC forces the SUT to produce, in a controlled way, rare outputs more frequently than their true probability of occurrence. The goal is that at each cycle a new segment of the PDF tail of the SUT output is estimated. In this subsection we give a behavioral description of our MMC platform. The algorithmic details are given in the Appendix.

Fig. 2 illustrates the block-diagram of the MMC platform. The MMC simulation consists of N_{MMC} MMC cycles. At each cycle N random vectors are serially generated by the random vector generator (RVG) unit. A random input vector is denoted by $\underline{X}$. The action of the SUT on the input vector is abstractly shown by a mapping g from the d-dimensional input space of random vectors to the one-dimensional output space of the test statistic Y. In this paper, SUT is the SS-WDM link equipped with the SOA, whose corresponding $g(\cdot)$ is described in the next subsection. The test statistic is the sampled voltage at the receiver. The input vector $\underline{X}$ has the following form:

$$\underline{X} \triangleq [\underline{E}; P] \tag{7}$$

$\underline{E}$ is a vector of independent, identically distributed, continuous random variables called the noise vector. P is a nonnegative integer between 0 and $2^M - 1$, where M is the SUT memory in terms of number of bit intervals. The binary representation of P is the bit pattern loaded in the SUT.

The noise vector is written as

$$\underline{E} \triangleq [\underline{A}; \underline{B}; C]. \tag{8}$$

The noise vector consists of two subvectors, $\underline{A}$, and, $\underline{B}$, and one scalar C. Subvector $\underline{A}$ contains random variables used to synthesize the input spectrum sliced random process. Subvector $\underline{B}$ is passed to the SOA model inside the SUT to simulate the spontaneous emission events in the SOA. It contains samples of the real and imaginary parts of $\epsilon(z,t)$ [see (1) and (5) and Section III-C] at all sampled space-time points. The scalar C represents the receiver thermal noise voltage.

At the first MMC cycle, the elements of $\underline{E}$ are independent Gaussian random variables with zero mean and unit variance.[1] P is distributed uniformly among integers between 0 and $2^M - 1$. At each cycle, after all samples are generated and passed to the SUT, the histogram of outputs is formed. The histogram calculated in cycle k is denoted by $\hat{H}_Y^{(k)}$. The PDF estimate of Y is updated and denoted by $\hat{p}_Y^{(k)}$. At each cycle, the PDF warper unit uses the latest PDF update, calculated at the end of the previous

[1]More precisely, element C is not actually zero mean, but rather its mean is selected to match measurements.

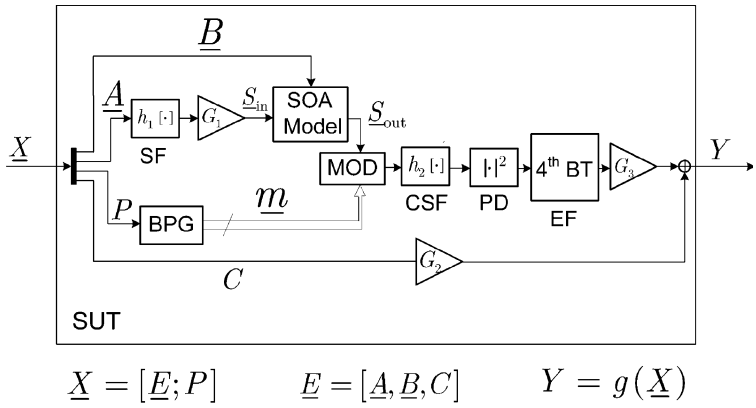

Fig. 3. Model of the SS-WDM link of Fig. 1 as a SUT inside the MMC platform of Fig. 2; BPG, bit pattern generator, MOD, modulator, SF, slicing filter, CSF, channel selecting filter, PD, photodetector, EF, electrical filter; 4th BT stands for fourth-order (lowpass) Bessel Thompson. Gain blocks are explained in the text.

cycle, to warp the PDF of the random input vectors $\underline{X}$ such that the corresponding output values are a driven toward rare events. The first MMC cycle is an MC simulation of the SUT. In subsequent cycles, the joint PDF of the spectrum sliced light, SOA amplified spontaneous emission (ASE), the receiver noise, and the bit pattern, represented respectively through $\underline{A}, \underline{B}, C$, and P, is warped and the PDF of Y is estimated down to very low probabilities. At the last cycle, the latest PDF update, $\hat{p}_Y^{(N_{\mathrm{MMC}})}(\cdot)$, is output and the simulator stops.

To estimate the BER, conditional PDFs of marks, $\hat{p}_Y^{(N_{\mathrm{MMC}})}(y\,|\,1)$, and spaces, $\hat{p}_Y^{(N_{\mathrm{MMC}})}(y\,|\,0)$, are separately estimated, and the area under the crossing tails is computed to yield the BER. The details of all the subsystems of the MMC platform of Fig. 2 are explained in the Appendix. The SUT is discussed in the next subsection.

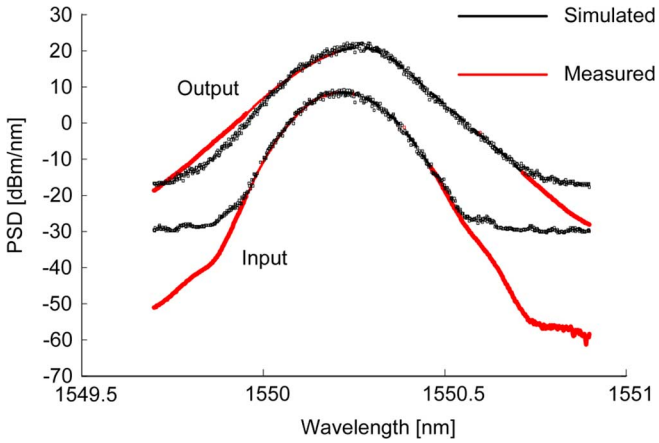

Fig. 4. Measured and simulated spectrum slices at the SOA input and output.

B. System Model

The block-diagram of the SUT is shown in Fig. 3. This block diagram corresponds to the SS-WDM link of Fig. 1. At the input, the random vector $\underline{X}$ is decomposed into its subcomponents: $\underline{A}, \underline{B}$, and C. The gain parameter G_1 is used to set the average input power to the SOA, since all filters in the simulator are normalized such that the vector of the impulse response has unit norm. G_2, and G_3 are used to adjust the noise and received signal power, respectively.

We model the thermal light source as having a lowpass equivalent optical field that is a complex Gaussian random process [11]. Experimentally, the BBS used had a 33.580 nm 3 dB bandwidth, as directly measured by the optical spectrum analyzer. In our SS-WDM experiment we filtered this BBS source using a 0.24 nm optical slicing filter (SF). Experimentally the BBS spectrum is flat over the narrow band of the slicing filter; thus, we model the output optical field of the BBS in the time domain by a white complex Gaussian noise, and filter it by our simulator's digital version of the SF. The output light will be partially coherent, with temporal coherence determined by the SF.

To synthesize the slicing filter, we measured the optical spectrum from the setup in Fig. 1, and then used the Remez exchange method, implemented in MATLAB, to extract the tap weights of an equivalent FIR filter, $h_1[\cdot]$, whose frequency response matches the measured optical spectrum after the slicing filter (see Fig. 1). The spectrum-sliced optical field is then obtained by filtering a complex white Gaussian noise by $h_1[\cdot]$. Fig. 4 shows the measured and simulated optical spectra at the SOA input and output.

Fig. 4 shows measured and simulated PSDs of optical fields both at the input and output of the SOA. The excellent correspondence of the measurement and simulation of the output light over the band of interest confirms that we have well modeled the coherency introduced by filtering, and validates our use of ideal, incoherent light as an input to the MMC simulator.

The SOA model is discussed in the next subsection. As illustrated in Fig. 4, we have chosen h_1 such that the measured and simulated spectrum slices match over a 30 dB range, which is sufficiently accurate for the simulations of this paper. The FIR filter had 10 taps. Matching over wider bandwidths can be achieved, if needed, at the expense of increasing the number of taps. The binary pattern generator (BPG) subsystem accepts the integer P, and outputs a vector $\underline{m}$, which is the binary representation of P. The modulator (MOD) subsystem shapes and upsamples bits $\underline{m}$, and adjusts the extinction ratio of the modulating waveform, for instance to match the experimental values, and finally multiplies the modulating waveform by the output vector of the SOA model.

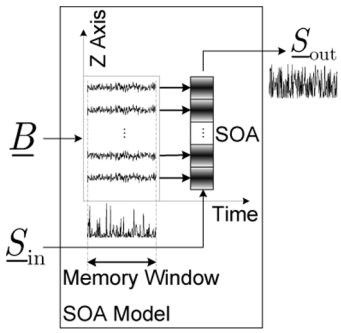

Fig. 5. Input-output definition of the SOA spatially resolved model.

The optical channel selecting filter (CSF) is modeled similarly to the SF, and the impulse response of its digital equivalent is $h_2[\cdot]$. The equivalent FIR filters synthesized by the Remez method have flat group delay. We verified that SF and CSF filters used experimentally also have flat group delay over their passbands. The photodetector (PD) is an ideal square-law element, and the electrical filter (EF) is obtained as the bilinear implementation of an analog fourth-order low-pass Bessel–Thompson filter [39].

C. SOA Model

Our SOA model is based on the method suggested in [35], where authors treat the propagation equation for the optical power as a stochastic differential equation in z, and apply second-order Runge–Kutta to solve it. We adapted the propagation solver of [35] to the optical field, added carrier dependent and independent loss coefficients (essential for satisfactory fit to experiments), and complemented it with an efficient solver of the dynamic gain equation. Here we discuss how the SOA model fits, as a subsystem, into the simulator.

The behavioral block diagram of the SOA model, as a subsystem in Fig. 3, is depicted in Fig. 5. We denote by M the memory of the link in terms of number of bits. Optical and electrical filters and dispersive elements contribute to system memory. A premodulator SOA does not contribute to the memory while a postmodulator SOA with a carrier lifetime comparable to the modulation bandwidth enhances the memory through the patterning effect.

We suppose each bit is upsampled N_s times. To calculate the SUT output at each instant, the past MN_s time samples (called the memory window) of the input waveform are needed. Since all waveforms are in the complex lowpass equivalent form, the length of $\underline{A}$ is $2MN_s$. In the spatially-resolved SOA model that is used, the SOA cavity is divided into N_{sec} sections. The spontaneous emission generated in each section over the memory window contributes to the SOA output. Subvector $\underline{B}$ contains samples of spontaneous emission events affecting the SUT output and it has $2MN_sN_{\text{sec}}$ elements; the factor 2 exists because $\epsilon(z,t)$ in (5) is a complex quantity. Given that C is a single element, the dimension of the input random vector is

$$d = 2MN_s + 2MN_sN_{\text{sec}} + 1. \tag{9}$$

IV. Results

In this section, we report our numerical and experimental results on statistical properties of the SS-WDM received signals in the presence of a nonlinear SOA and the CSF. Fig. 6 shows the experimental and simulated PDFs of the received voltage of the SS-WDM when a premodulator SOA was employed and the SOA input was a CW signal. The slicing filter (SF) was 0.24 nm wide, and CSF was identical to SF. The electrical filter bandwidth was 1.87 GHz. The DC-coupled receiver was an Agilent sampling scope. The power to voltage conversion ratio was 0.75 V/W.

Fig. 6(a) is the PDF of the SOA output without electrical filtering. This PDF in fact corresponds to the light intensity at the SOA output; since the slice bandwidth was 30 GHz, and the photodetector bandwidth was 50 GHz, the distortion induced by the finite bandwidth PD was not significant. The receiver noise standard deviation, when the optical input was turned off, was 8.8 μV as read from the scope. Fig. 6(b) corresponds to when a CSF is placed after SOA, but no electrical filtering is applied. In Fig. 6(c) the internal electrical filter of the sampling scope (bandwidth 1.87 GHz) is applied, but the CSF is removed. In Fig. 6(d) both CSF and electrical filter are present.

We can see that in all receiver configurations the fit of MMC and experiment is quite satisfactory. The major conclusions from Fig. 6 are that 1) the link model is accurate enough to generate valid statistics, and 2) the MMC platform provides PDF estimation down to very low probabilities with reasonable computation time.

In all cases, the average optical power input to SOA was 0 dBm, corresponding to deep saturation, and the bias current was 495 mA. Optical attenuators at SOA output were used to ensure the receiver electronics is not damaged. Adding optical and electrical filters led to extra insertion losses. We did not separately characterized the insertion losses of optical and electrical filters; instead, in each measurement, we recorded the sampled waveforms together with the histogram, and calculated the waveform mean voltage. Since the receiver noise had been separately characterized, we could account for the losses in our simulation. In each case, we manually set the histogram window of the scope, and recorded their limit values. These numbers, together with the length of the measured histogram, were used to define the output bins in simulations. The MMC simulations consisted of five cycles, and at each cycle 10^6 random vectors were generated. The SOA was divided into 50 sections, and the simulation time-step was 4 ps. The slowest simulation [Fig. 6(d)] took 1.5 h per MMC cycle.

To compute the BERs we need to estimate the conditional PDFs of marks and spaces. We have to set the SUT memory in the MMC simulator, and estimate PDFs of marks and spaces separately. To find the system memory, we performed a set of MMC simulations, with increasing values of the system memory, and continued the simulations until the PDF estimates converged. Fig. 7(a) shows the PDF estimates at the last cycle in three separate MMC simulations with increasing M, when the SOA is placed before the modulator. The small mismatch in the tails is due to the ISI introduced by the electrical filter. Although not the focus of our paper, the case in which the SOA

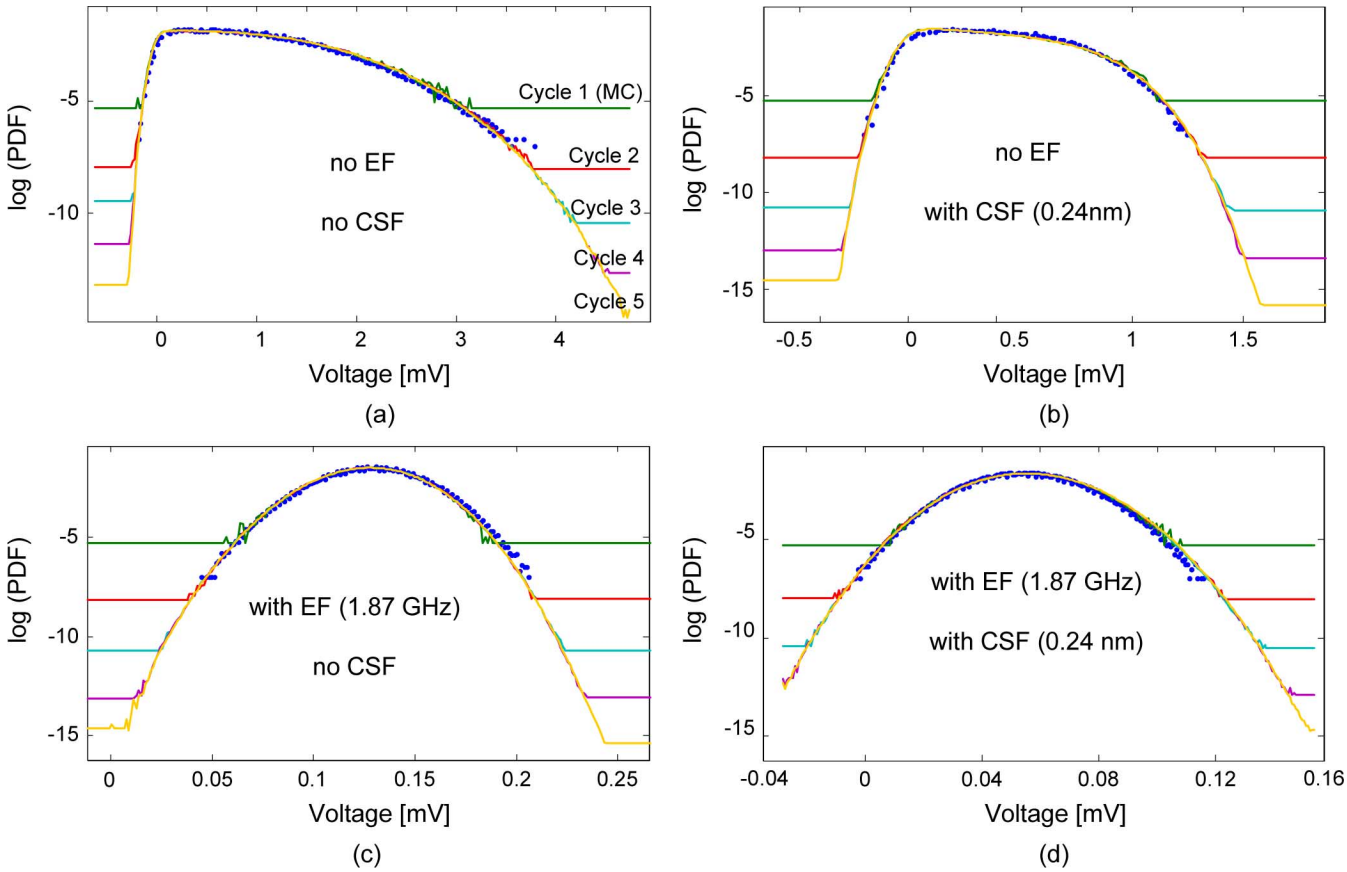

Fig. 6. Measured (dots) and simulated PDFs of the received voltage in a SS-WDM link equipped with premodulator nonlinear SOA, (a) no electrical filter, no CSF, (b) no electrical filter, with CSF, (c) electrical filter of bandwidth 1.87 GHz, no CSF, and (d) electrical filter at 1.87 GHz and CSF.

follows the modulator provides an interesting contrast in the PDF of marks, as shown in Fig. 7(b). In the postmodulator case much larger ISI is visible in the multimodal structure of the "true" PDF, obtained by increasing the system memory up to $M = 4$. Note that for $M = 1$ the MMC routine is not able to reproduce the second ISI-induced mark "rail" on the eye diagram, and, thus, a single-mode PDF is produced, much as in Fig. 7(a). In the case of Fig. 7(b), the bit-rate was set to 2.5 Gb/s, and the SOA carrier lifetime was set to one bit duration, i.e., 400 ps. Note this is faster response than the SOA we characterized and used in our premodulator measurements with 170 ps lifetime. The extinction ratio was set to 20 dB to exaggerate the patterning effect. The conclusion of Fig. 7(b) is that our simulation tool can capture a possible link memory enhancement due to SOA nonlinear operation.

To predict the BER of our SS-WDM link equipped with premodulator SOA-based noise suppression, we set the SUT memory to $M = 2$. Fig. 8 shows the conditional PDFs on both marks and spaces at a received power of -8 dBm in the following cases: (a) with neither SOA nor CSF (label "SS-WDM"); (b) with noise cleaning SOA but without CSF (label "SOA"); (c) with both SOA and CSF (label "SOA and CSF"). In each case, the BER at optimal threshold is the area under the crossing tails of the conditional PDFs. Both BER improvement due to SOA noise cleaning, and BER degradation due to postfiltering are visible in Fig. 8. In this example, the BER degradation ensuing from postfiltering is not severe, due to the rather low linewidth enhancement factor ($\alpha = 3.5$). We next compare simulated BERs with measured BERs. The measured conversion ratio of the Agilent 11982A PD was 320 V/W. The extinction ratio of the external Mach–Zehnder modulator was used as a fitting parameter to match the floors of SS-WDM BER curves; an 11.2 dB extinction ratio was used in all simulations. For simulated BERs we swept the input power, found the optimal threshold (intersection of conditional PDFs), and calculated the BER from the conditional PDFs. Both 1.25 Gb/s and 2.5 Gb/s BERs were investigated. Fig. 9 reports both measured and simulated BERs for the three cases already illustrated in Fig. 8. The receiver and BERT noises were characterized using the techniques discussed in [40]. We note the excellent match between MMC simulation and experiments, clearly illustrating the performance estimation accuracy of the MMC method when a reliable simulator of the SUT is available.

Finally, we comment on possible extensions of the presented work. The SOA model used in this study included neither SOA ultrafast processes nor polarization effects. Neglecting ultrafast dynamics is justified for SS-WDM, as the optical field input to the SOA has a narrow linewidth (0.24 nm) set by the SF. The signal variations at the SOA input are much slower than typical time constants of carrier heating and spectral hole burning [41]; hence, we neglected these processes in our study. By replacing the present SOA model with one of the well-known models that include ultrafast dynamics, we could investigate these effects.

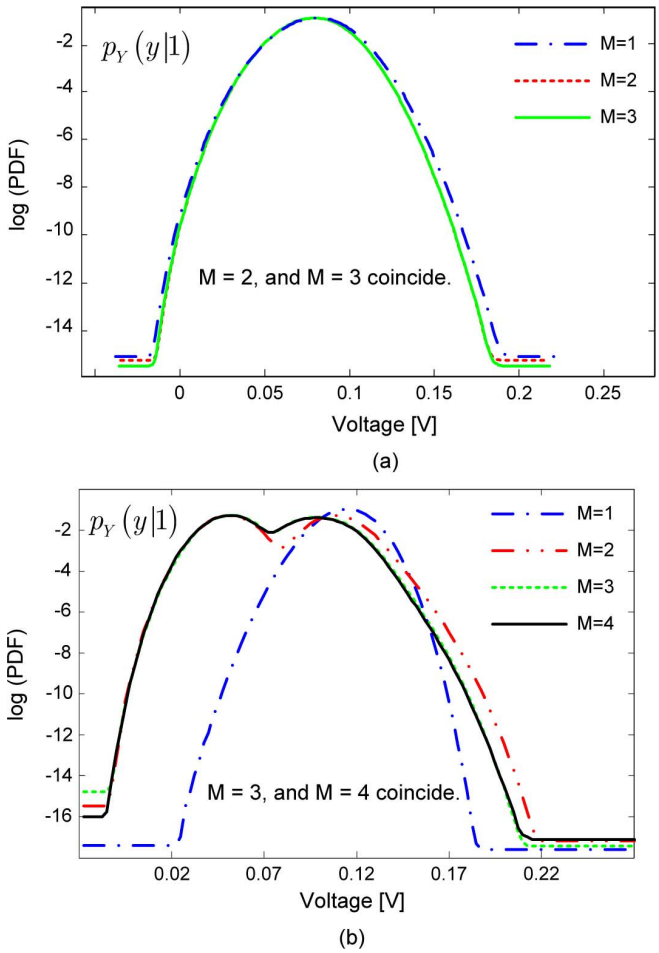

Fig. 7. Simulated PDF of marks corresponding to different values of system memory. (a) The premodulator setup with the parameters coming from the experiment. (b) The postmodulator setup with a hypothetical SOA slower than what we used in the measurements.

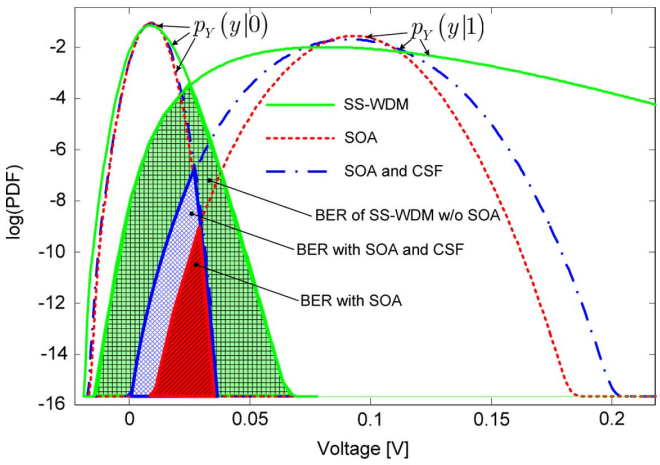

Fig. 8. Simulated conditional PDFs of marks and spaces corresponding to: SS-WDM (label "SS-WDM"), SS-WDM with premodulator SOA (label "SOA"), and SS-WDM with premodulator SOA and CSF (label "SOA and CSF").

Similarly, neglecting polarization effects was not critical for our experimental validation. We used a polarization beam splitter after the BBS, and controlled the polarization state of the light

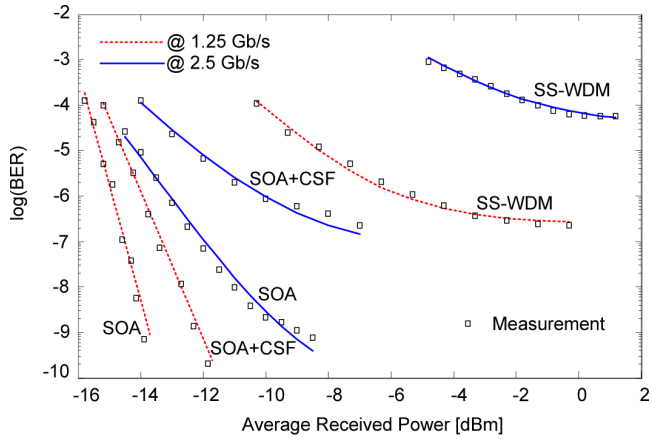

Fig. 9. Measured and simulated BERs.

both at the input of the SOA, and at the MZM input using polarization controllers. The measurements were recorded after adjusting the SOA input polarization for maximum gain. The impact of cross polarization on the light statistics can be studied by replacing the SOA model in our simulator with a one including polarization effects, e.g., [42], and enlarging the input vector space to produce random input vectors for TE, and TM polarization states.

V. Conclusion

In this paper, we described a simulation tool to evaluate the performance of optical links employing nonlinear SOAs. We applied our simulator to study noise mitigation of SS-WDM systems by a premodulator SOA. We modeled the broadband source, slicing, channel selecting, and electrical filters all in time domain. We used a spatially-resolved SOA model including distributed carrier dependent, and carrier independent loss mechanisms and ASE. We completed the standard MMC simulation algorithm with a fast and efficient pattern warping technique to capture the ISI. We showed that both the statistics of the CW slices, and the BERs at various bit-rates can be predicted with our simulation tool. In particular, we are able to quantify the impact of receiver optical filtering effect on system performance. The simulator can be useful as a design tool to optimize SS-WDM systems, as well as studying various SOA-based regenerative systems.

Appendix

Our goal in this Appendix is to provide sufficient detail for other researchers to make use of our simulation tool. We will present in broad outlines the techniques we have exploited in our simulator, without going into detailed development. In the following, we first give a general description of the MMC technique, then we give details of various subsystems.

The SUT is represented by an abstract mapping $g(\cdot)$ from an input space to an output space. The elements of the input space are vectors $\underline{X}$ with a known PDF $p_{\underline{X}}(\underline{X})$, possibly with an unknown normalization constant [27]. We are interested in estimating, by simulation, the unknown probability mass function (PMF) of the SUT output, p_Y, over a prespecified set of

output space bins that extend down to the tail. The multicanonical Monte Carlo (MMC) is an adaptive importance-sampling technique aiming to solve this problem by adapting to a flat histogram of the output samples. All flat histogram methods share the basic idea that given a limited number of output realizations, the best one can do to estimate the probability of a series of events is to evenly distribute the samples over those events. In our case, the events are SUT output bins.

We suppose the output space is divided into N_{bins} bins indexed by integer $b = 1, \ldots, N_{\text{bins}}$. The MMC cycle number is denoted by $k = 1, \ldots, N_{\text{MMC}}$, where N_{MMC} is the number of MMC cycles. The PMF estimate obtained at the end of the kth cycle is denoted by $\hat{p}_Y^{(k)}$. The output PMF is initialized to

$$\hat{p}_Y^{(0)}[b] = \frac{1}{N}; \quad b = 1, \ldots, N_{\text{bins}} \tag{10}$$

where N is the number of samples generated per MMC cycle. We denote the ith input sample, generated within the kth cycle by $\underline{X}_i^{(k)}$. The corresponding output sample is $Y_i^{(k)} = g(\underline{X}_i^{(k)})$, with $i = 1, \ldots, N$. The normalized histogram of the set of output samples over the prespecified output bins is denoted by $\hat{H}_Y^{(k)}$.

The strategy of MMC is to first perform a "short" MC simulation, during which a set of input samples $\{\underline{X}_1^{(1)}, \ldots, \underline{X}_N^{(1)}\}$ with the known PDF $p_{\underline{X}}(\underline{X})$ is generated, the corresponding set of output values $\{Y_1^{(1)}, \ldots, Y_N^{(1)}\}$ is obtained, and a first estimate $\hat{p}_Y^{(1)}$ of the PMF of the output random variable Y is formed. Then the first cycle is finished. In the second cycle, the input samples $\{\underline{X}_1^{(2)}, \ldots, \underline{X}_N^{(2)}\}$ are generated such that their distribution follows the following *warped* PDF:

$$\pi^{(1)} \triangleq C_1 \frac{p_{\underline{X}}(\underline{X})}{\hat{p}_Y^{(1)}[\text{bin}(g(\underline{X}))]} \tag{11}$$

where C_1 is a nomalization factor, and the "bin" function returns the bin index of output samples. Drawing input samples from the input warped PDF in (11) forces output samples to fall more on the tail than on the mode, so that $\hat{H}_Y^{(2)}$ will be flatter than $\hat{H}_Y^{(1)}$. Cycles continue until the output histogram is sufficiently flat, that is, when the unwarped output PDF has been estimated to sufficient precision in the tails to achieve the simulation goals (e.g., down to a $\text{BER} = 10^{-12}$.). Then $\hat{p}_Y^{(N_{\text{MMC}})}[b]$ is output for all bins b and MMC simulation stops.

Having described the MMC algorithm we proceed to discuss the various subsystems. Fig. 10 shows the details of the subsystems of the MMC platform block diagram of Fig. 2. We have divided the MMC platform into four basic subsystems, i.e., PDF warper, random vector generator (RVG), histogram update, and PDF update. We briefly discuss each subsystem here.

We start with the PDF warper subsystem, the most important subsystem of the MMC platform. The adaptation in the MMC approach requires generation of realizations in the multidimensional input space following the statistics of the very irregular multidimensional warped PDF that is fixed for the cycle, see (11). We refer to the warped PDF of the kth cycle by $\pi^{(k)}$. The input realizations (or samples) are generated using a Markov chain Monte Carlo (MCMC) technique known as

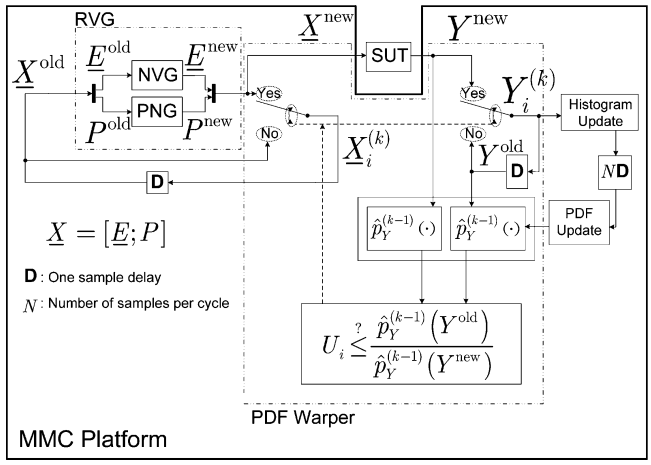

Fig. 10. Detailed block-diagram of the MMC platform. RVG: random vector generator, NVG: noise vector generator, PNG: pattern number generator, SUT: system under test, D represents unit delay.

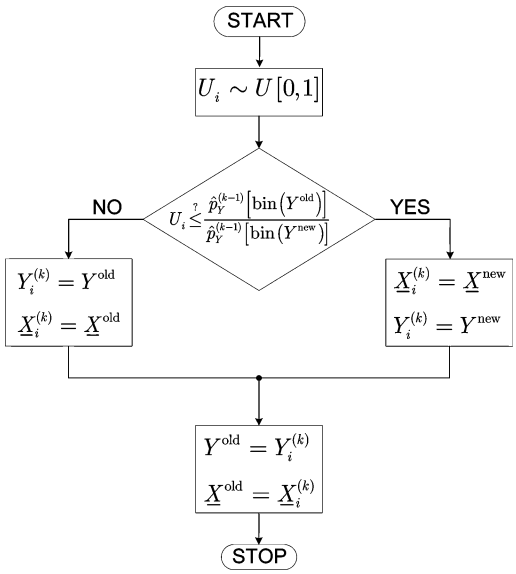

Fig. 11. Flowchart of the PDF Warper. $U[0, 1]$ is a uniform RV on [0,1].

Metropolis-Hastings. The idea is to propose input samples according to their unwarped distribution $p_{\underline{X}}(\underline{X})$, which is known, regular and well-behaved, and then either reject or accept the proposed samples (rejection means that the previous realization is reused) per a specified, randomized criterion. Proposal of new samples is done by RVG, and will be discussed later. The resulting dependent sequence of samples from $p_{\underline{X}}(\underline{X})$ will asymptotically have the desired warped PDF $\pi^{(k)}$, provided proper selection of the randomized rejection criterion. For an entire cycle, a Metropolis-Hastings MCMC algorithm runs within the (input) PDF warper. The flowchart of the PDF warper is shown in Fig. 11.

Now we consider RVG. The RVG uses Markov chain Monte Carlo (MCMC) techniques to facilitate the generation of samples by the RVG, as illustrated in the flowchart in Fig. 12. The Metropolis-Hastings MCMC techniques were used in the PDF warper as the warped distribution is not well behaved. The RVG uses MCMC to instead favor generation of samples in restrained

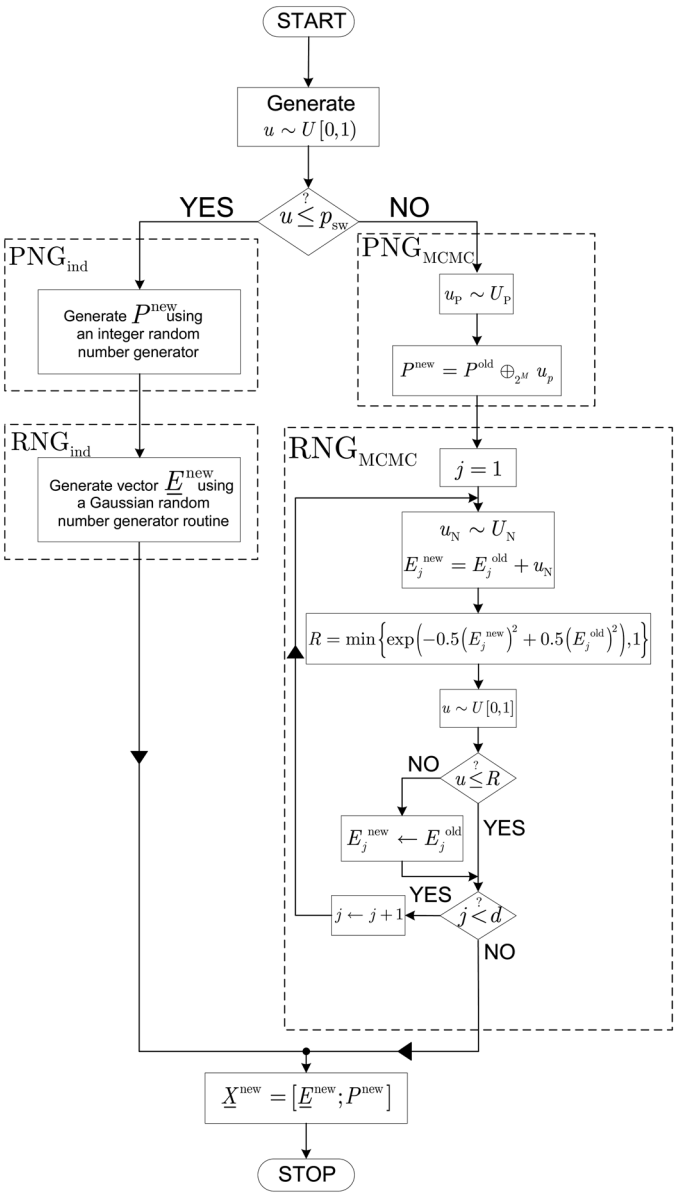

Fig. 12. Flowchart of the RVG.

subsets of the input space. The simulator can, thus, explore a certain area of the output space in greater detail, instead of covering the entire area in a more "willy-nilly" fashion. While the proposed input vectors are now correlated, the net effect is to lead to a better overall convergence of the MMC adaptation. Consider first the PNG. PNG generates P uniformly distributed over the set of integers $\{0, \ldots, 2^M - 1\}$. With probability p_{sw} an independent sample P^{new} is generated (using $\mathrm{PNG}_{\mathrm{ind}}$), while with probability $1 - p_{sw}$ the sample is constrained to fall in a certain neighborhood of the old sample P^{old} [44]. We used p_{sw} of 0.1 in our simulations. $\mathrm{PNG}_{\mathrm{ind}}$ calls a standard random integer generator routine to generate the new proposal independent from the past. On the other hand, given P^{old}, $\mathrm{PNG}_{\mathrm{MCMC}}$ proposes a new pattern through $P^{\mathrm{new}} = P^{\mathrm{old}} \oplus_{2^M} u_p$, where $\oplus_{2^M}$ denotes modulo 2^M addition. The innovation u_p is constrained to permit only a limited number of bits to flip. u_p is a zero-mean, discrete, uniformly distributed random variable taking integer values from $-M_p$ to M_p. In our simulations, we used $M_p = 1$, i.e., from pattern M we go either to $M+1$, or to $M-1$, or to M.

Consider next the RNG which generates a vector of Gaussian random variables. With probability p_{sw} a sample $\underline{E}^{\mathrm{new}}$ of independent, identically distributed zero-mean, unit variance Gaussian elements is generated (using $\mathrm{RNG}_{\mathrm{ind}}$), while with probability $1 - p_{sw}$ the sample is either constrained to fall in a certain neighborhood of the old sample $\underline{E}^{\mathrm{old}}$ or $\underline{E}^{\mathrm{new}}$ is simply recycled (using $\mathrm{RNG}_{\mathrm{MCMC}}$). $\mathrm{RNG}_{\mathrm{MCMC}}$ consists of d independent Markov chains. Each chain generates an innovation u_N that is uniformly distributed over $[-M_N, M_N]$. We used $M_N = 1.5$ in our simulations. Note that parameters p_{sw}, M_p, and M_N were chosen by trial and error. With probability R the previous sample $\underline{E}^{\mathrm{old}}$ is reused with no innovation where

$$R = \min\left(\exp\left(-0.5\left(E_j^{\mathrm{new}}\right)^2 + 0.5\left(E_j^{\mathrm{old}}\right)^2\right), 1\right). \quad (12)$$

With probability $1 - R$, the innovation is added to the previous sample$\underline{E}^{\mathrm{old}}$ to generate the $\underline{E}^{\mathrm{new}}$. The RVG flowchart is given in Fig. 12.

Having now described all the component parts, we give in Fig. 13 the overall flowchart of the MMC algorithm and discuss how the input warped pdf is generated after each cycle.

The histogram update subsystem collects accepted output samples and calculates $\hat{H}_Y^{(k)}$, over the output bins. We assume $\hat{H}_Y^{(k)}[b]$ represents the number of outputs found in the b'th bin at the end of cycle k, normalized by the total number of iterations N.

The PDF update subsystem uses $\hat{H}_Y^{(k)}$ and the latest output PDF estimate to make a new estimate; $\hat{p}_Y^{(k)}[b]$ is the new probability that the output will fall in the b'th bin. The probability of the first bin is $\hat{p}_Y^{(k)}[1] = \hat{p}_Y^{(k-1)}[1]$, and we then use [31], [27]

$$\frac{\hat{p}_Y^{(k)}[b+1]}{\hat{p}_Y^{(k)}[b]} = \frac{\hat{p}_Y^{(k-1)}[b+1]}{\hat{p}_Y^{(k-1)}[b]} \left[\frac{\hat{H}_Y^{(k)}[b+1]}{\hat{H}_Y^{(k)}[b]}\right]^{\hat{g}_k[b]} \quad b \in [1, \ldots, N_{\mathrm{bins}}] \quad (13)$$

where

$$\tilde{g}_k[b] = \frac{\hat{H}_Y^{(k)}[b]\hat{H}_Y^{(k)}[b+1]}{\hat{H}_Y^{(k)}[b] + \hat{H}_Y^{(k)}[b+1]} \quad (14)$$

and

$$\hat{g}_k[b] = \frac{\tilde{g}_k[b]}{\sum_{s=1}^{k} \tilde{g}_s[b]} \quad (15)$$

The resulting PMF $\hat{p}_Y^{(k)}$ is normalized to assure the total probability is one.[2]

Finally, we note that the PDF warper does not calculate (11) directly to achieve warping. In fact the warping exploits the ratio $\pi^{(k)}(Y^{\mathrm{new}})/\pi^{(k)}(Y^{\mathrm{old}})$. This ratio reduces to

$$\frac{\hat{p}_Y^{(k-1)}[\mathrm{bin}(Y^{\mathrm{old}})]}{\hat{p}_Y^{(k-1)}[\mathrm{bin}(Y^{\mathrm{new}})]} \quad (16)$$

[2] $\tilde{g}$ and $\hat{g}$ should not be confused with the SUT mapping $g(\cdot)$.

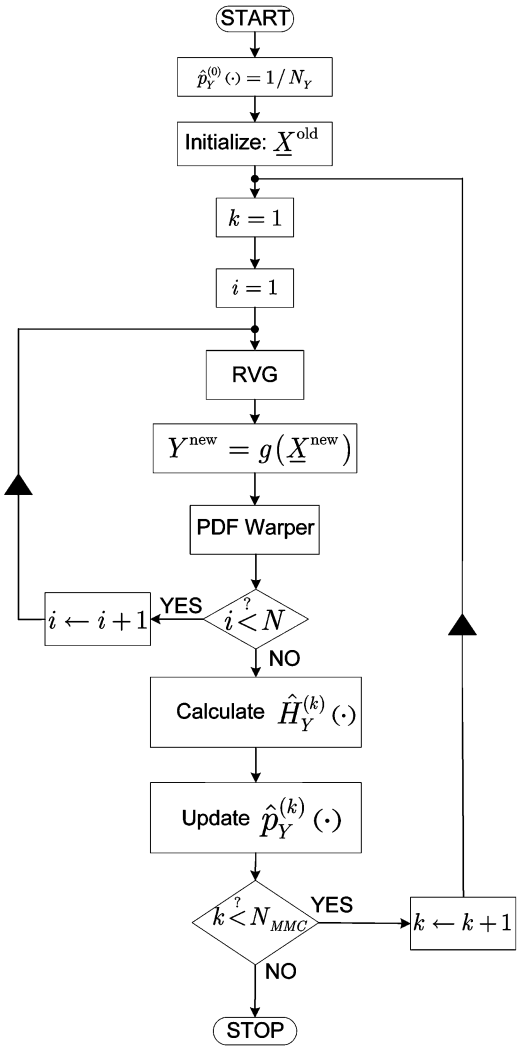

Fig. 13. Flowchart of the MMC.

so that the normalization constants for the warped PDF need never be found—an extremely desirable characteristic of the MMC algorithm for high-dimensional inputs such as ours.

REFERENCES

[1] Y. Katagiri, K. Suzuki, and K. Aida, "Intensity stabilisation of spectrum-sliced Gaussian radiation based on amplitude squeezing using semiconductor optical amplifiers with gain saturation," *Electron. Lett.*, vol. 35, pp. 1362–1364, 1999.

[2] S. J. Kim, J. H. Han, J. S. Lee, and C. S. Park, "Intensity noise suppression in spectrum-sliced incoherent light communication systems using a gain-saturated semiconductor optical amplifier," *IEEE Photon. Technol. Lett.*, vol. 11, pp. 1042–1044, 1999.

[3] M. Zhao, G. Morthier, R. Baets, and J. Dekoster, "Investigation of the intensity noise reduction using a saturated semiconductor optical amplifier in spectrum sliced WDM systems," *CLEO*, pp. 383–384, 2001.

[4] M. Zhao, G. Morthier, and R. Baets, "Analysis and optimization of intensity noise reduction in spectrum-sliced WDM systems using a saturated semiconductor optical amplifier," *IEEE Photon. Technol. Lett.*, vol. 14, pp. 390–392, 2002.

[5] T. Yamatoya and F. Koyama, "Noise suppression of spectrum-sliced light using semiconductor optical amplifiers," *Electron. Commun. Jpn. Part 2*, vol. 86, pp. 28–35, 2003.

[6] T. Yamatoya and F. Koyama, "Optical preamplifier using optical modulation of amplified spontaneous emission in saturated semiconductor optical amplifier," *J. Lightw. Technol.*, vol. 22, pp. 1290–1295, 2004.

[7] T.-Y. Kim, "Intensity noise suppression of 2.5 Gb/s spectrum-sliced incoherent signal using a gain-saturated SOA injected by broadband light," *OECC*, pp. 46–47, 2004.

[8] D. Forsyth, "Spectrum-sliced broadband source intensity noise reduction using semiconductor optical amplifier nonlinear gain compression," *Proc. SPIE*, vol. 5825, pp. 448–454, 2005.

[9] F. Koyama and H. Uenohara, "Noise suppression and optical ASE modulation in saturated semiconductor optical amplifiers," in *Proc. 38th Asilomar Conf. Signals, Systems and Computers*, 2004, vol. 1, pp. 198–202.

[10] A. D. McCoy, B. C. Thomsen, M. Ibsen, and D. J. Richardson, "Filtering effects in a spectrum-sliced WDM system using SOA-based noise reduction," *IEEE Photon. Technol. Lett.*, vol. 16, pp. 680–682, 2004.

[11] A. D. McCoy, P. Horak, B. C. Thomsen, M. Ibsen, and D. J. Richardson, "Noise suppression of incoherent light using a gain-saturated SOA: Implications for spectrum-sliced WDM systems," *J. Lightw. Technol.*, vol. 23, pp. 2399–2409, 2005.

[12] A. D. McCoy, P. Horak, M. Ibsen, and D. J. Richardson, "Performance comparison of spectrum-slicing techniques employing SOA-based noise suppression at the transmitter or receiver," *IEEE Photon. Technol. Lett.*, vol. 18, pp. 1494–1496, 2006.

[13] P. R. Morkel, R. I. Laming, H. O. Edwards, and D. N. Payne, "Elimination of excess photon noise from fiber super-radiant sources," *CLEO 90*, pp. 154–155, 1990.

[14] A. J. Keating, W. T. Holloway, and D. D. Sampson, "," *IEEE Photon. Technol. Lett.*, vol. 7, pp. 1513–1515, 1995.

[15] J. Han, J. W. Ko, J. S. Lee, and S. Y. Shin, "0.1-nm narrow bandwidth transmission of a 2.5-Gb/s spectrum-sliced incoherent light channel using an all-optical bandwidth expansion technique at the receiver," 1998, vol. 10, pp. 1501–1503.

[16] F. Ohman, S. Bischoff, B. Tromborg, and J. Mork, "Noise and regeneration in semiconductor waveguides with saturable gain and absorption," *IEEE J. Quant. Electron.*, vol. 40, pp. 245–255, 2004.

[17] T. Vivero, N. Calabretta, I. Tafur, Monroy, G. Carvalho, Kassar, F. Ohman, K. Yvind, A. Gonzalez-Marcos, and J. Mork, "10 Gb/s-NRZ optical 2R-regeneration in two-section SOA-EA chip," *LEOS*, pp. 806–807, 2007.

[18] K. Sato and H. Toba, "Reduction of mode partition noise by using semiconductor optical amplifiers," *IEEE J. Sel. Topics Quant. Electron.*, vol. 7, pp. 328–333, 2001.

[19] E. Desurvire, *Erbium-Doped Fiber Amplifiers, Principles and Applications*. New York: Wiley-Interscience, 2002.

[20] M. Shtaif, B. Tromborg, and G. Eisenstein, "Noise spectra of semiconductor optical amplifiers: Relation between semiclassical and quantum descriptions," *IEEE J. Quant. Electron.*, vol. 34, pp. 869–878, 1998.

[21] F. Ohman, J. Mork, and B. Tromborg, "Output power PDF of a saturated semiconductor optical amplifier: Second-order noise contributions by path integral method," *IEEE J. Quant. Electron.*, vol. 43, pp. 1188–1197, 2007.

[22] A. A. M. Saleh and I. M. I. Habbab, "Effects of semiconductor-optical-amplifier nonlinearity on the performance of high-speed intensity-modulation lightwave systems," *IEEE Trans. Commun.*, vol. 38, pp. 839–846, 1990.

[23] G. J. Foschini, G. Vannucci, and L. J. Greenstein, "Envelope statistics for filtered optical signals corrupted by phase noise," *IEEE Trans. Commun.*, vol. 37, pp. 1293–1302, 1989.

[24] E. Forestieri, "Evaluating the error probability in lightwave systems with chromatic dispersion, arbitrary pulse shape and pre- and postdetection filtering," *J. Lightw. Technol.*, vol. 18, pp. 1493–1503, 2000.

[25] M. C. Jeruchim, "Techniques for estimating the bit error rate in the simulation of digital communication systems," *J. Sel. Areas. Commun.*, vol. SAC-2, pp. 153–170, 1984.

[26] G. P. Agrawal and N. A. Olsson, "Self-phase modulation and spectral broadening of optical pulses in semiconductor laser amplifiers," *IEEE J. Quant. Electron.*, vol. 25, pp. 2297–2306, 1989.

[27] B. A. Berg, "Introduction to multicanonical monte carlo simulations," *Fields Instrum. Commun.*, vol. 26, no. 1, pp. 1–24, 2000, (also available at arXiv:cond-mat/9909236v1).

[28] D. Yevick, "Multicanonical communication system modeling-application to PMD statistics," *IEEE Photon. Technol. Lett.*, vol. 14, pp. 1512–1514, 2002.

[29] D. Yevick and T. Lu, "Improved multicanonical algorithms," *J. Opt. Soc. Amer. A*, vol. 23, pp. 2912–2918, 2006.

[30] T. Lu, D. O. Yevick, L. Yan, B. Zhang, and A. E. Willner, "An experimental approach to multicanonical sampling," *IEEE Photon. Technol. Lett.*, vol. 16, pp. 1978–1980, 2004.

[31] R. Holzlohner and C. R. Menyuk, "Use of multicanonical Monte Carlo simulations to obtain accurate bit error rates in optical communications systems," *Opt. Lett.*, vol. 28, no. 20, pp. 1894–1896, Oct. 2003.
[32] A. O. Lima and C. R. Menyuk, "Error estimation in multicanonical Monte Carlo simulations with applications to polarization-mode-dispersion emulators," *J. Lightw. Technol.*, vol. 23, pp. 3781–3789, 2005.
[33] W. Pellegrini, J. Zweck, C. R. Menyuk, and R. Holzlohner, "Computation of bit error ratios for a dense WDM system using the noise covariance matrix and multicanonical Monte Carlo methods," *IEEE Photon. Technol. Lett.*, vol. 17, pp. 1644–1646, 2005.
[34] Y. Yadin, M. Shtaif, and M. Orenstein, "Bit-error rate of optical DPSK in fiber systems by multicanonical Monte Carlo simulations," *IEEE Photon. Technol. Lett.*, vol. 17, pp. 1355–1357, 2005.
[35] A. Bilenca and G. Eisenstein, "Statistical noise properties of an optical pulse propagating in a nonlinear semiconductor optical amplifier," *IEEE J. Quant. Electron.*, vol. 41, pp. 36–44, 2005.
[36] A. Bilenca and G. Eisenstein, "Fokker-planck and langevin analyses of noise accompanying the amplification of optical pulses in semiconductor optical amplifiers," *J. Opt. Soc. Amer. B*, vol. 22, pp. 1632–1639, 2005.
[37] J. W. Goodman, *Statistical Optics*. New York: Wiley, 1985.
[38] M. J. Connelly, "Wide-band steady-state numerical model and parameter extraction of a tensile-strained bulk semiconductor optical amplifier," *IEEE J. Quant. Electron.*, vol. 43, pp. 47–56, 2007.
[39] M. C. Jeruchim, P. Balaban, and K. S. Shanmugan, *Simulation of Communication Systems*, 2nd ed. Boston, MA: Kluwer, 2000.
[40] S. Ayotte, M. Rochette, J. Magne, L. A. Rusch, and S. LaRochelle, "Experimental verification and capacity prediction of FE-OCDMA using superimposed FBG," *J. Lightw. Technol.*, vol. 23, pp. 724–731, 2005.
[41] A. Mecozzi and J. Mork, "Saturation effects in nondegenerate four-wave mixing between short optical pulses in semiconductor laser amplifiers," *IEEE J. Sel. Topics Quant. Electron.*, vol. 3, pp. 1190–1207, 1997.
[42] H. J. S. Dorren, D. Lenstra, L. Yong, M. T. Hill, and G.-D. Khoe, "Nonlinear polarization rotation in semiconductor optical amplifiers: Theory and application to all-optical flip-flop memories," *IEEE J. Quant. Electron.*, vol. 39, pp. 141–148, 2003.
[43] B. A. Berg and T. Neuhaus, "Multicanonical ensemble: A new approach to simulate first-order phase transitions," *Phys. Rev. Lett.*, vol. 68, p. 9, 1992.
[44] Y. Guan, R. Fleissner, P. Joyce, and S. M. Krone, "Markov chain monte carlo in small worlds," *Statist. Comput.*, vol. 16, no. 2, pp. 193–202, 2006.

Amirhossein Ghazisaeidi received the M.A. degree in communications systems and the B.S. degree in electrical engineering from the Sharif University of Technology, Tehran, Iran. He is currently pursuing the Ph.D. degree in the ECE Department, Laval University, Quebec, Canada.

His research interests include optical-code-division multiple access and spectrum sliced WDM using incoherent sources, dynamics, and noise properties of optical amplifiers, modeling optoelectronic devices, and performance analysis of optical links.

Francesco Vacondio was born in Reggio Emilia, Italy, in 1981. In October 2006, he received the "Laurea Magistrale" degree (*cum laude*) in telecommunications engineering from the University of Parma, Parma, Italy.

Since September 2005, he has been with the Department of Electrical and Computer Engineering, Universit Laval, Quebec, Canada, where his research interests include semiconductor optical amplifiers, phase modulated formats, and microwave photonics.

Alberto Bononi received the Laurea degree in electronics engineering (*cum laude*) from the University of Pisa, Italy, in 1988, and the M.A. and Ph.D. degrees in electrical engineering from Princeton University, Princeton, NJ, 1992, and 1994, respectively.

Currently, he is an Associate Professor of telecommunications at the School of Engineering, Università di Parma, Italy. He teaches courses in probability theory and stochastic processes, telecommunications networks, and optical communications. In 1990, he was with the GEC-Marconi Hirst Research Centre, Wembley, U.K., on a Marconi S.p.A. project on coherent optical systems. From 1994 to 1996, he was an Assistant Professor in the Electrical and Computer Engineering Department, State University of New York (SUNY), Buffalo, teaching courses in electric circuits and optical networks. In the summers of 1997 and 1999, he was a Visiting Faculty at the Département de Genie Électrique, Université Laval, QC, Canada, doing research on fiber amplifiers. His present research interests include system design and performance analysis of high-speed all-optical networks, nonlinear fiber transmission for WDM systems, linear and nonlinear polarization mode dispersion, and transient gain dynamics in optical amplifiers.

Leslie Ann Rusch (S'91–M'94–SM'00) received the B.S.E.E. (honors) degree from the California Institute of Technology, Pasadena, in 1980, and the M.A. and Ph.D. degrees in electrical engineering from Princeton University, Princeton, NJ, in 1992 and 1994, respectively.

In 1994, she joined the Department of Electrical and Computer Engineering, Universit Laval, Qubec, QC, Canada, where she is currently a Full Professor performing research in wireless and optical communications. She spent two years as the manager of a group researching new wireless technologies at Intel Corp. from 2001 to 2002. Her research interests include optical-code-division multiple access and spectrum sliced WDM using incoherent sources for passive optical networks; semiconductor and erbium-doped optical amplifiers and their dynamics; radio over fiber; and in wireless communications, high performance, reduced complexity receivers for ultrawideband systems employing optical processing.